Computer Simulation of Ruthenium Complexes Molecules: Density Functional Theory Study of Ruthenium Tris Chelate Complexes

Peiyuan Li [a,b], Wei Su [a,*], Jianguo Cui [a], Lini Huo [a], Nana Guo [a], Yanmin Huang [a]

[a]College of Chemistry and Life Science, Guangxi Teachers Education University, Nanning 530001,China

[b]College of Pharmacy, Guangxi Traditional Chinese Medical University,Nanning 530001,China

Abstract. Density functional theory (DFT) calculations were carried out to comparatively describe the molecular structures, atomic charges, molecular orbital energies, and infrared (IR) spectra of six ruthenium complexes containing different number of 2,2ʹbipyridine (bpy) and salicylaldehyde thiosemicarbazone (H3saltsc) ligands, [Ru(bpy)x(H2saltsc)3-x], Ru(bpy)32+ (1), Ru(bpy)2(H2saltsc)+ (2), Ru(bpy) (H2saltsc)2 (3, 4), Ru(H2saltsc)3- (5, 6). The calculated structural data of compounds 1, 2 and the simulated electronic absorption and IR spectra of 1 are compared with X-ray crystallography molecular structures, IR spectra respectively, and good consistencies between the calculated and experimental results are found. The molecular orbital energies of compounds 1-6 shifted to higher energy level as the number of H3saltsc ligands increases due to the electron-donating properties of H3saltsc, indicating the complexes with more H3saltsc ligands may possess more potential to be employed as bioredox drug. The effects of different axial ligands on the structures and properties of the series of ruthenium complexes are also described in detail.

Keywords: Density functional calculations; Ruthenium complex; IR spectra

1. Introduction

In the recent decades, ruthenium complexes offer much potential in the design of pharmaceuticals for their remarkable biological activities [1]-[2]. Some of these compounds exhibit prominent anticancer activity, for example, the complex $(H_2im)[trans-RuCl_4-(Him)(DMSO)]$ (NAMI-A), as an efficient anti-metastatic drug [3]-[4], and $(H_2Ind)[trans-RuCl_4-(Hind)2]$ (KP1019), as an anticancer drug, have reached the phase I clinical trials [5]-[6] and stimulated much interest in the medicinal properties of these complexes.

Among the numerous ligands that have been employed in ruthenium complexes, 2,2ʹbipyridine (bpy) and salicylaldehyde thiosemicarbazone (H3saltsc) attract more and more attention [7]. The ruthenium complexes containing salicylaldehyde thiosemicarbazone ligands, with the conjugated N–N–S tridentate ligand system, display outstanding bioinorganic and biological activities (viz. antiprotozoal [8], antibacterial [9], antitumor activities [10]-[12]. On the other hand, tris(2,2ʹbipyridine)-ruthenium(II) $[Ru(bpy)_3^{2+}]$ and its derivatives show DNA-binding properties and then have been extensively employed in biosensors [13] and biological probes [14-15]. Besides, the ruthenium complex with one salicylaldehyde thiosemicarbazone and two 2,2ʹbipyridine ligands, namely $[Ru(bpy)_2(H_2saltsc)]^+$, has been prepared and expected to display some interesting properties by Bhattacharya et al [16]-[17]. However, there are still relatively few investigations for ruthenium complexes containing the ligands 2,2ʹbipyridine and salicylaldehyde thiosemicarbazone in either experiments or theoretic calculations despite the potential applications of these complexes as medicines.

Herein we describe molecular structures, atomic charges, molecular orbital energy, electronic absorption and IR spectra of $[Ru(bpy)_x(H_2saltsc)_{3-x}]^{x-1}$ (x = 3, 2, 1, 0) {$Ru(bpy)_3^{2+}$ (**1**), $Ru(bpy)_2(H_2saltsc)^+$ (**2**), Ru(bpy) $(H_2saltsc)_2$ (**3, 4**), Ru $(H_2saltsc)_3^-$ (**5, 6**)} in detail with DFT calculations using the B3LYP [18] functional and

---

the LANL2DZ [19-20] /6-31G(d) basis set. The calculated structures of $[Ru(bpy)_3]^{2+}$ and $[Ru(bpy)_2(H_2saltsc)]^+$, and the simulated UV-vis and IR spectra of $Ru(bpy)_3^{2+}$ are compared with the reported experimental results. The effects of different axial ligands to the structures and properties of a series of ruthenium complexes are also described.

2. Computational Details

The hybrid density functional B3LYP (Becke-Lee-Young-Parr composite of exchange-correlation functional) method11 was used for both geometry optimizations and property calculations of $[Ru(bpy)x(H_2saltsc)3-x]x-1$ (x = 3, 2, 1, 0) (1-6). In all cases, the LANL2DZ basis set [19]-[20] was used for Ru atom and 6-31G(d) basis set for other atoms. Using the energy-minimized structures generated in the previous step, normal coordinate analyses were carried out. Charge distribution is carried out using a full natural bond orbital analysis (NBO) population method16 based on the minimized structure with Gaussian NBO 3.1 in the Gaussian 03 program [21]. Electronic absorption spectroscopic calculations were performed by TDDFT method. All calculations were carried out using the Gaussian 03 program in the [21] IBM P690 system in Shandong Province High Performance Computing Centre.

3. Results and Discussion

3.1. Molecular Structures

The calculated structures of $Ru(bpy)_3^{2+}$ (1), $Ru(bpy)_2(H_2saltsc)^+$ (2), $Ru(bpy) (H_2saltsc)_2$ (3, 4), Ru $(H_2saltsc)^{3-}$ (5, 6) are shown in Fig. 1. The $H_2saltsc$ ligand is coordinated to ruthenium as a bidentate N,S donor in a four-membered chelate ring [22]. It is noteworthy that the fact that no imaginary vibration is predicted in the following frequency calculations of the IR vibration spectroscopy indicates that the energy minimized structures for all of the six complexes are true energy minima.

The calculated structure parameters of $Ru(bpy)_3^{2+}$ (1) and $Ru(bpy)_2(H_2saltsc)^+$ (2) are compared with the X-ray crystallography data in Table 1. As can be seen, the biggest differences in bond length between the calculated and experimental data for compounds 1 and 2 are only 0.062 Å for $Ru-N_1$ and 0.073 Å for $Ru-S_1$, respectively; and the smallest one is merely 0.040 Å for $Ru-N_4$ in compound 2, indicating that the results obtained from the DFT B3LYP method with LANL2DZ/6-31G (d) basis set correspond very well with the experimental data. The biggest differences in bond angles between the simulated and experimental results come from $N1-Ru-N_2$ with the departure of 1.0 ° and 1.2 ° for compounds 1 and 2 respectively, whereas the smallest difference is from N_3-Ru-N_4 in compound 2 with a nearly coincident value, 0.5 °. As was mentioned by many other investigators26, the bond angle has a much larger error than the bond length in the molecular simulation. This situation also exists in the present case as is clearly shown in Table 1. However, the error is very small compared with that in other papers [23]. Again, the good agreement between the structural data obtained by the DFT method and the experimental results for compounds 1 and 2 indicates that our calculation method is reliable for simulating these large complexes.
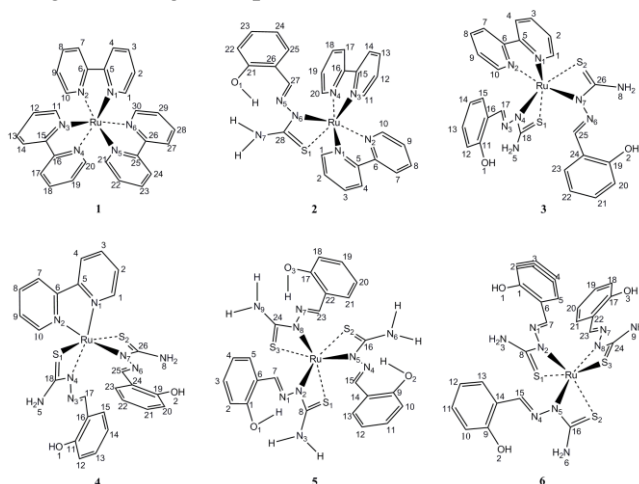

Fig. 1. Calculated structures of molecule 1-6

The calculated main bond lengths and bond angles of compounds 1-6 are shown in Table 2. The bipyridine ligand is a symmetric bidentate ligand, which binds to ruthenium ion as a bidentate N,N donor in a five-membered chelate ring. $Ru(bpy)_3^{2+}$ (1) alternates along the 3-fold axis of the unit cell, with identical metric features of 2.118 Å. For compounds 2, one salicylaldehyde thiosemicarbazone ligand is coordinated to ruthenium as a bidentate N, S donor in a four-membered chelate ring with a bite angle of 66.2 °, and the lengths of Ru-N and Ru-S coordination bond with salicylaldehyde thiosemicarbazone are 2.169 Å and 2.506 Å, respectively. While one more bipyridine ligand is replaced by a salicylaldehyde thiosemicarbazone ligand, the structure parameters of the remaining bipyridine ligands are slightly mutative, i.e., the bite angles of bipyridine ligand change in the range of ±0.2 °, and the bond lengths of Ru-N (N on the bipyridine ligand) decrease to 2.088~2.110 Å. For compounds 3 and 4, the bite angles of bipyridine ligand increase to 78.6° while the bond lengths slump to 2.058 ~ 2.078 Å. For compounds 5 and 6, the bite angles are approximately 65.2 °, and the lengths of Ru-N and Ru-S are 2.134~2.173 Å and 2.541~2.569 Å, respectively. In short, the bite angles of bipyridine and ruthenium ion increase while the bond lengths of Ru-N decrease with increasing amounts of salicylaldehyde thiosemicarbazone ligands.

TABLE 1. EXPERIMENTAL AND CALCULATED MAIN STRUCTURAL PARAMETER OF MOLECULE 1 AND 2

Molecule 1	Experimental [a]	Calculated	Molecule 2	Experimental [b]	Calculated
$Ru-N_1$	2.056	2.118	$Ru-N_1$	2.027	2.088
$Ru-N_2$	2.056	2.118	$Ru-N_2$	2.033	2.103
$Ru-N_3$	2.056	2.118	$Ru-N_3$	2.054	2.106
$Ru-N_4$	2.056	2.118	$Ru-N_4$	2.070	2.110
$Ru-N_5$	2.056	2.118	$Ru-N_6$	2.099	2.169
$Ru-N_6$	2.056	2.118	$Ru-S_1$	2.432	2.506
N_1-Ru-N_2	78.7	77.7	N_1-Ru-N_2	76.7	77.9
N_3-Ru-N_4	78.7	77.7	N_3-Ru-N_4	78.0	77.5
N_5-Ru-N_6	78.7	77.7	S_1-Ru-N_6	66.8	66.2

[a] Data taken from Ref. [23], [b] Data taken from Ref. [17].

TABLE 2. THE CALCULATED MAIN BONDS LENGTHS (Å) AND BOND ANGLES (O) OF MOLECULE 1-6

1	2	3	4	5	6
$Ru-N_1$ (2.118)	$Ru-N_1$ (2.088)	$Ru-N_1$ (2.058)	$Ru-N_1$ (2.062)	$Ru-N_2$ (2.135)	$Ru-N_2$ (2.160)
$Ru-N_2$ (2.118)	$Ru-N_2$ (2.103)	$Ru-N_2$ (2.078)	$Ru-N_2$ (2.062)	$Ru-S_1$ (2.568)	$Ru-S_1$ (2.547)
$Ru-N_3$ (2.118)	$Ru-N_3$ (2.106)	$Ru-N_4$ (2.151)	$Ru-N_4$ (2.181)	$Ru-N_5$ (2.135)	$Ru-N_5$ (2.143)
$Ru-N_4$ (2.118)	$Ru-N_4$ (2.110)	$Ru-S_1$ (2.545)	$Ru-S_1$ (2.524)	$Ru-S_2$ (2.567)	$Ru-S_2$ (2.555)
$Ru-N_5$ (2.118)	$Ru-N_6$ (2.169)	$Ru-N_7$ (2.161)	$Ru-N_7$ (2.181)	$Ru-N_8$ (2.134)	$Ru-N_8$ (2.174)
$Ru-N_6$ (2.118)	$Ru-S_1$ (2.506)	$Ru-S_2$ (2.512)	$Ru-S_2$ (2.524)	$Ru-S_3$ (2.569)	$Ru-S_3$ (2.541)
N_1-Ru-N_2(77.7)	N_1-Ru-N_2(77.9)	N_1-Ru-N_2(78.6)	N_1-Ru-N_2(78.6)	N_2-Ru-S_1(65.2)	N_2-Ru-S_1(65.3)
N_3-Ru-N_4(77.7)	N_3-Ru-N_4(77.5)	N_4-Ru-S_1(65.6)	N_4-Ru-S_1(65.6)	N_5-Ru-S_2(65.2)	N_5-Ru-S_2(65.3)
N_5-Ru-N_6(77.7)	N_6-Ru-S_1(66.2)	N_7-Ru-S_2(65.6)	N_7-Ru-S_2(65.6)	N_8-Ru-S_3(65.2)	N_8-Ru-S_3(65.2)

coordinated to ruthenium as a bidentate N, S donor in a four-membered chelate ring with a bite angle of 66.2°, and the lengths of Ru-N and Ru-S coordination bond with salicylaldehyde thiosemicarbazone are 2.169 Å and 2.506 Å, respectively. While one more bipyridine ligand is replaced by a salicylaldehyde thiosemicarbazone ligand, the structure parameters of the remaining bipyridine ligands are slightly mutative, i.e., the bite angles of bipyridine ligand change in the range of ±0.2°, and the bond lengths of Ru-N (N on the bipyridine ligand) decrease to 2.088~2.110 Å. For compounds **3** and **4**, the bite angles of bipyridine ligand increase to 78.6° while the bond lengths slump to 2.058~2.078 Å. For compounds **5** and **6**, the bite angles are approximately 65.2°, and the lengths of Ru-N and Ru-S are 2.134~2.173 Å and 2.541~2.569 Å, respectively. In short, the bite angles of bipyridine and ruthenium ion increase while the bond lengths of Ru-N decrease with increasing amounts of salicylaldehyde thiosemicarbazone ligands.

3.2. Molecular Orbital Energies

The calculated energies of the molecular orbitals from HOMO-5 to LUMO+5 of compounds 1-6 are shown in Fig. 2. From compounds 1 to 6, the HOMO and LUMO are shifted to higher energy levels as the number of salicylaldehyde thiosemicarbazone ligands increases in the mixed-ligand complexes due to the π-donor properties of salicylaldehyde thiosemicarbazone ligands. The increase of the energy of HOMO leads to a smaller ionization potential. Compound 1, the metal complexes with the most bipyridine ligands, has much lower molecular orbital energy than the other five complexes, indicating it possesses the largest ionization potential caused by the strong electron-withdrawing property of bipyridine ligands. It is known that HOMO energy can be determined from the first oxidation w aves in cyclic voltammograms. According to the calculated results, the HOMO energy levels of molecule 1 and 2 are -11.032 and -7.203 eV, corresponding with the oxidation potential (Eox) value (vs. SCE), at +1.354 and +0.62 V, respectively. There is a trend that the Eox lowers with increasing calculated HOMO energy lever value. Consequently, it can be deduced that Eox of molecule 3-6 will keep on decreasing from 3 to 6. For ruthenium antitumor drugs, an appropriate redox potential is probably a more important parameter than cytotoxic potency under normal conditions. The lower the Eox is, the less difficult the molecule to be oxidized in aqueous solution at pH 7.31 As a result, compounds 3-6 might possess more potential to be employed as bioredox drugs.
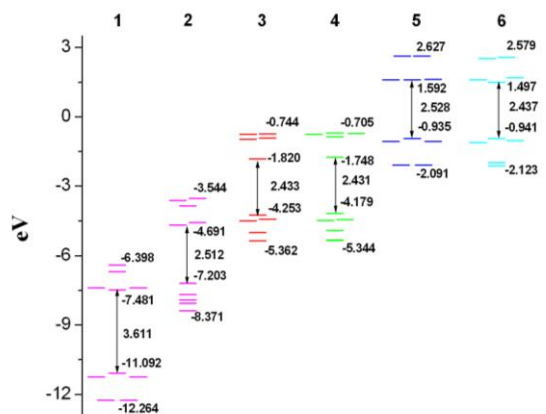

Fig. 2. Orbital energies of the HOMO, LUMO orbital of 1–6

It should be mentioned that the absolute value of the orbital energy gaps have no practical meanings because DFT methods significantly underestimate orbital gaps due the incorrect 1/r behavior of the standard exchange functional. But the calculated values can still be used to compare with the other complexes in the same group because the same method and basis set are used throughout. As is shown in Fig. 2, the energy gaps from HOMO to LUMO of compound **1** (3.611 eV) is the largest in all molecules, which makes compound **1** the most stable in all the six complexes. The values of other compounds are in the range from 2.431 to 2.528 eV, and the minor difference of the gap energy of compounds **2-6** indicates that these five complexes have comparable stability. It is noteworthy that the values of HOMO–LUMO gap for these ruthenium complexes are very important for getting information of their electronic absorptions, which reflect the energy necessary for the transition of an electron from the HOMO to the LUMO and therefore should correlate with the lowest energy optical transition in the electronic absorption spectrum.

3.3. Electronic absorption Spectra

According to the experimental results, six main absorption bands appear at 451, 345, 323, 285, 250 and 238 nm in the UV-vis spectra of **1** in H_2O as solvent. A diminutive deviation is found between the calculated and experimental results due to the solvent effect. The calculated absorption band at 308 nm is corresponding to the observed high-energy absorption band at 285 nm, which is assigned as $\pi \rightarrow \pi^*$ transitions. Corresponding to the observed bands at 451, 345 and 323 nm, there are four absorption bands at 417, 402, 341 and 323 nm according to our calculation, which were all attributed to the $d \rightarrow \pi^*$ transition.

Just in line with the molecular orbital energy calculation results described above, the absorption bands of compounds **2**-**6** appear at the lower energy side than that of compound **1**, indicating that these complexes (**2**-**6**) have more potential application in photoelectrochemical cell. However, the absorption bands of **2**-**6** locate at the similar region because of their close orbital energy gap. The assignments of the UV-vis spectra bands for these complexes have been made by comparison with the reported spectra of analogue. The detailed spectra are expected to be more complicated for complexes **2**-**6**, because of multiple charge-transfer transitions, which may result from lower-symmetry splitting of the metal level, the presence of different acceptor orbitals and the mixing of singlet and triplet configurations in the excited state through spin-orbit coupling (Fig. 2). For complexes **2**-**6**, coordination of salicylaldehyde thiosemicarbazone is via N,S atoms and the bands at 394, 390, 392, 390, and 397 nm respectively, may be assigned to $n \rightarrow \pi^*$ transitions centered on the C=N moiety. And other bands appear in the visible region (in the region of 400-700 nm) in spectra of complexes **2**-**6**, which are attributed to $d \rightarrow \pi^*$ transitions.

3.4. Infrared spectra

Normal coordinate analyses have been performed based on the minimum-energy geometries of all complexes. The calculated infrared spectra of **1**-**6** are shown in Fig. 3. The ν(Ru-N, Ru-S) bands of the six complexes are in the region ~430 cm^{-1}, that is, 437 cm^{-1} for **1**; 432 cm^{-1} for **2**; 418 and cm^{-1} for **3**; 409 and 385 cm^{-1} for **4**; 453, 413 and 393 cm^{-1} for **5**; 450, 411 and 392 cm^{-1} for **6**. The vibrational bands of the ligands containing bipyridine and salicylaldehyde thiosemicarbazone are discussed in detail as following.

The spectra of compounds **1**-**4**, which are all including bipyridine ligand, are similar at many peaks. For Ru(bpy)$_3^{2+}$ (**1**), only three weak peaks at 3251, 3242 and 3224 cm^{-1} are observed above 3000 cm^{-1}, which are totally C-H stretching according to our calculation, with assistance of animated pictures produced based on the normal coordinates. The peaks at 1651 cm^{-1} for **1**, 1663 and 1643 cm^{-1} for **2**, for **3**, 1660 and 1634 cm^{-1} for **4**, are contributed by C-H in plane bending and C-C stretching vibration. At the region from 1550 to 1450 cm^{-1}, there are three peaks at 1510, 1490 and 1472 cm^{-1} for **1**, which are the mixture of C-H in plane bending and bipyridine C-C and C-N stretching vibration. The peaks at 785 and 750 cm^{-1} for **1** are C-H out-of-plane bending, and the corresponding peak red-shifts to 780 and 748 cm^{-1} for **2** (at the blue shift of the shoulder peaks at 772 and 740 cm^{-1} for **3**, 771 and 739 cm^{-1} for **4**).
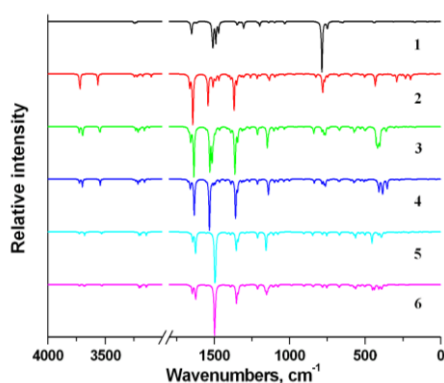
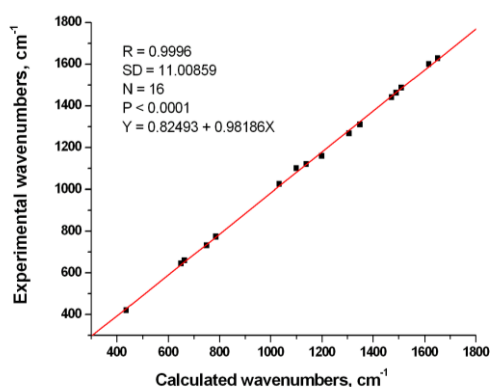

Fig. 3. Simulated IR spectra of molecule 1-6

Fig. 4. Consistency of the wavenumbers of the main peaks in calculated and experimental IR spectra of molecule 1. (R: Correlation coefficient; SD: Standard deviation of the fit; N: Number of data points; P: Probability that R is zero)

The infrared spectra of compounds **5** and **6** are also shown in Fig. 3. The peaks at 3680 cm^{-1} for **6**, 3679 cm^{-1} for **5**, 3698 cm^{-1} for **3** and **4**, 3719 cm^{-1} for **2**, taking a blue-shift trend, are totally N-H symmetry stretching, and the peaks at 3530 cm^{-1} for **6**, also blue-shift to 3532 cm^{-1} for **5**, 3546 cm^{-1} for **4** and **3**, 3566 cm^{-1} for **2**, are due to N-H asymmetry stretching vibration. The strongest peak appears at 1499 cm^{-1} for **6** and 1496 cm^{-1} for **5**, are at the red side of corresponding peak at 1532 cm^{-1} for **4**, 1530 cm^{-1} for **3** and 1542 cm^{-1} for **2**, indicating the shift trend that it takes blue shift with decreasing salicylaldehyde thiosemicarbazone group amount.

To ensure the calculated results, the calculated IR spectra of compound **1** are compared to the recorded experimentally in Fig. 4. The intuitional correspondence relationship of the calculated and experimental data was obtained by fitting them to a linear function. The slope of the line is 0.982 and the intercept only 0.825, showing good consistency between the calculated and experimental data. These results suggest that different scale factors for different vibration bands are needed in simulating the calculated IR spectrum. Usually, the scale factor found in the middle course was chosen as a general one used for simulation.

4. Conclusion

The molecular structures, atomic charges, molecular orbitals energy, UV-vis spectra and IR spectra of six ruthenium tris chelate complexes containing the ligands 2,2′-bipyridine and salicylaldehyde thiosemicarbazone have been calculated using DFT B3LYP method at the LANL2DZ/6-31G(d) level with Gaussian 03 program. By comparative study of the six complexes with different number of 2,2′-bipyridine and salicylaldehyde thiosemicarbazone ligands, it is found that the molecular orbitals energies shift to higher energy level as the number of salicylaldehyde thiosemicarbazone ligands increases in the series of complexes due to the π-donor properties of salicylaldehyde thiosemicarbazone ligand. The calculated structural data of compounds 1 and 2 and the IR spectra of 1 are compared with X-ray crystallography molecular structures and the experimental absorption spectra respectively, and well consistencies have been found, indicating the feasibility for calculating such a large molecule as ruthenium complexes. The differences between the geometric isomer are compared, and the infrared spectra of 1-6 are also explained and identified comparatively.

5. Acknowledgements

6. References

[1] Clarke MJ, Zhu F, Frasca DR. Non-platinum Chemotherapeutic Metallopharmaceuticals. *Chem Rev* 1999; **99**:2511–2533.

[2] Clarke MJ. Ruthenium metallopharmaceuticals. *Coord Chem Rev* 2002; **232**:69–93.

[3] Sava G, Gagliardi R, Bergamo A, Alessio E, Mestroni G. Treatment of metastases of solid mouse tumours by NAMI-A: comparison with cisplatin, cyclophosphamide and dacarbazine. *Anticancer Res* 1999; **19**:969–972.

[4] Groessl M, Reisner E, Hartinger CG, Eichinger R, Semenova O, Timerbaev AR, Jakupec MA, Arion VB, Keppler BK. Structure−Activity Relationships for NAMI-A-type Complexes (HL)[*trans*-RuCl₄L(*S*-dmso)ruthenate(III)] (L = Imidazole, Indazole, 1,2,4-Triazole, 4-Amino-1,2,4-triazole, and 1-Methyl-1,2,4-triazole): Aquation, Redox Properties, Protein Binding, and Antiproliferative Activity. *J Med Chem* 2007; **50**:2185–2193.

[5] Galanski M, Arion VB, Jakupec MA, Keppler BK. Recent Developments in the Field of Tumor-Inhibiting Metal Complexes. *Curr Pharm Des* 2003; **9**:2078–2089.

[6] Hartinger CG, Zorbas-Seifried S, Jakupec MA, Kynast B, Zorbas H, Keppler BK. From bench to bedside – preclinical and early clinical development of the anticancer agent indazolium trans-[tetrachlorobis(1H-indazole)ruthenate(III)] (KP1019 or FFC14A). *J Inorg Biochem* 2006; **100:**891–904.

[7] Dilovic I, Rubcic M, Vrdoljak V, Pavelic SK, Kralj M, Piantanidab I, Cindric M. Novel thiosemicarbazone derivatives as potential antitumor agents: Synthesis, physicochemical and structural properties, DNA interactions and antiproliferative activity. *Bioorg Med Chem* 2008; **16:**5189–5198.

[8] Singh S, Athar F, Maurya MR, Azam A. Cyclooctadiene Ru(II) complexes of thiophene-2-carboxaldehyde-derived thiosemicarbazones: synthesis, characterization and antiamoebic activity. *Eur J Med Chem* 2006; **41**:592–598,.

[9] Kannan S, Sivagamasundari M, Ramesh R, Liu Y. Ruthenium(II) carbonyl complexes of dehydroacetic acid thiosemicarbazone: Synthesis, structure, light emission and biological activity. *J Organomet Chem* 2008; **693**:2251–2257.

[10] Grguric-Sipka S, Kowol CR, Valiahdi SM, Eichinger R, Jakupec MA, Roller A, Shova S, Arion VB, Keppler BK. Ruthenium(II) Complexes of Thiosemicarbazones: The First Water-Soluble Complex with pH-Dependent Antiproliferative Activity. *Eur J Inorg Chem* 2007; 2870–2878.

[11] Lobana TS, Bawa G, Butcher RJ, Liu CW. Thiosemicarbazonates of Ruthenium(II): Crystal Structures of [Bis(triphenylphosphine)][bis(N-phenyl-pyridine-2-carbaldehyde Thiosemicarbazonato)]ruthenium(II) and [Bis(diphenylphosphino) butane][bis(salicylaldehyde Thiosemicarbazonato)] ruthenium(II). *Anorg Allg Chem* 2009; **635**:355–360.

[12] Kowol CR, Reisner E, Chiorescu I, Arion VB, Galanski M, Deubel DV, Keppler BK. An Electrochemical Study of Antineoplastic Gallium, Iron and Ruthenium Complexes with Redox Noninnocent α-N-Heterocyclic Chalcogensemicarbazones. *Inorg Chem* 2008; **47**:11032–11047.

[13] Liu J, Su B, Lagger G, Tacchini P, Girault HH. Antioxidant Redox Sensors Based on DNA Modified Carbon Screen-Printed Electrodes. *Anal. Chem.* 2006; **78**:6879–6884.

[14] Zeglis BM, Barton JK. Binding of Ru(bpy)$_2$(eilatin) $^{2+}$ to Matched and Mismatched DNA. *Inorg Chem* 2008; **47**:6452–6457.

[15] Augustyn KE, Stemp EDA, Barton JK. Charge Separation in a Ruthenium-Quencher Conjugate Bound to DNA. *Inorg Chem* 2007; **46**:9337–9350.

[16] Basuli F, Peng SM, Bhattacharya S. Unusual Coordination Mode of Thiosemicarbazone Ligands. A Search for the Origin. *Inorg Chem* 2000; **39**:1120–1127.

[17] Pal I, Basuli F, Mak TCW, Bhattacharya S. Synthesis, Structure, and Properties of a Novel Heterooctametallic Complex Containing a Cyclic Ru$_4$Ni$_4$ Core. *Angew Chem Int Ed* 2001; **40**:2923–2925.

[18] Becke AD. Density-functional thermochemistry. III. The role of exact exchange. *J Chem Phys* 1993; **98**:5648-5652.

[19] Hay PJ, Wadt WR. Ab initio effective core potentials for molecular calculations. Potentials for the transition metal atoms Sc to Hg. *J Chem Phys* 1985; **82**: 270–283.

[20] Wadt WR, Hay PJ. Ab initio effective core potentials for molecular calculations. Potentials for main group elements Na to Bi. *J Chem Phys* 1985; **82**:284–298.

[21] Frisch MJ, Trucks GW, Schlegel HB, Scuseria GE, Robb MA, Cheeseman JR,et.al.Gaussian 03, Revision B.05, Gaussian, Inc,Pittsburgh PA, 2003.

[22] Rillema D, Jones D, Levy H.Structure of tris(2,2'-bipyridyl)ruthenium(II)hexafluorophosphate, [Ru(bipy)$_3$][PF$_6$]$_2$;X-ray crystallographic determination. *J C S Chem Comm*1979;849–851.

[23] Zhang Y, Zhang X, Liu Z, Bian Y, Jiang J. Structures and Properties of 1,8,15,22-TetrasubstitutedPhthalocyaninato-Lead Complexes:The Substitutional Effect StudyBased on Density Functional Theory Calculations. *J Phys Chem A* 2005; **109**:6363–6370.